Journal of Computational and Applied Mathematics 234 (2010) 2213–2221

Contents lists available at ScienceDirect

Journal of Computational and Applied Mathematics

journal homepage: www.elsevier.com/locate/cam

# Limit analysis decomposition and finite element mixed method

Franck Pastor [a,*], Etienne Loute [b]

[a] Laboratoire de Mécanique de Lille, UMR-CNRS, Université des Sciences et Technologies de Lille, 59 655 Villeneuve d'Asq, France

[b] Facultés universitaires Saint-Louis and Louvain School of Management, bld. Jardin Botanique 43, 1000 Brussels, Belgium

ARTICLE INFO

*Article history:*
Received 8 September 2008
Received in revised form 29 January 2009

*Keywords:*
Porous material
Convex optimization
Decomposition
Limit analysis
Finite element method
Mixed approach

ABSTRACT

This paper proposes an original decomposition approach to the upper bound method of limit analysis. It is based on a mixed finite element approach and on a convex interior point solver, using linear or quadratic discontinuous velocity fields. Presented in plane strain, this method appears to be rapidly convergent, as verified in the Tresca compressed bar problem in the linear velocity case. Then, using discontinuous quadratic velocity fields, the method is applied to the celebrated problem of the stability factor of a Tresca vertical slope: the upper bound is lowered to 3.7776 – value to be compared to the best published lower bound 3.7752 – by succeeding in solving a nonlinear optimization problem with millions of variables and constraints.



## 1. Introduction

Limit Analysis theory is concerned in finding the limit loadings of mechanical systems by classically using two separated approaches, the static one involving only stress tensors as variables, the second, or kinematic approach, using only displacement velocities. The static method gives a lower bound to the limit loading, the kinematic one an upper bound. Less used, a third approach involving both variables – velocities as virtual variables and stresses as real variables – generally gives an approximation of the limit loading. However, the status of the final result is not defined in terms of bounds, except for some particular cases of involved fields of variables. All these methods result numerically in constrained optimization problems solved until recently by Linear Programming (LP) after linearizing the nonlinear conditions. In the last decade, powerful algorithms – as the so-called interior point methods – have allowed to solve directly the original, nonlinear problems. Recently, an interior point optimization solver was presented in [1] and improved in [2] for solving the static problems for homogeneous Gurson materials – where conic programming does not apply – and for von Mises materials. Henceforth, this optimization solver, fully detailed in [3], will be called IP-OPT.

To our knowledge, the first mixed approaches were proposed in [4,5] for continuous velocity fields and piecewise linear criteria, and for general conditions in [6,7]. A novel mixed formulation, which uses convexity properties to provide rigorous kinematical solutions with discontinuous quadratic velocity fields, was proposed in [8] and detailed in [3,9]. The corresponding finite element formulation appears to be very efficient, because of the robustness of the IP-OPT solver, which can solve very large problems when commercial conic codes fail to converge. Nevertheless, for heterogeneous materials or for obtaining very precise bounds, more refined meshes are needed. As a consequence, the size of the numerical problems becomes too large. In the following, after a very short summary of the algorithm implemented in the optimization solver, we briefly review the variational formulation and the resulting mixed method. Then we present the proposed decomposition approach in plane strain and its detailed application to the compressed bar between rough dies and to the classical – still not entirely solved – problem of the stability of a vertical slope in a Tresca (or von Mises) material.

* Corresponding address: Laboratoire de Mecanique de Lille, Universite Catholique de Louvain, CESAME, 4 av. Georges Lemaitre, Bat Euler, 1348 Louvain-la-Neuve, Belgium.
*E-mail addresses:* franck.pastor@skynet.be (F. Pastor), loute@fusl.ac.be (E. Loute).

0377-0427/$ – see front matter © 2009 Elsevier B.V. All rights reserved.
doi:10.1016/j.cam.2009.08.074

## 2. Limit Analysis and variational formulation

For the sake of clarity, without any loss in generality, we consider that the velocity fields are continuous.

### 2.1. Reminder of LA

According to Salençon (see [10]), a stress tensor field $\sigma$ is said to be statically admissible (SA) if equilibrium equations, stress vector continuity, and stress boundary conditions are verified. It is said to be plastically admissible (PA) if $f(\sigma) \leqslant 0$, where $f(\sigma)$ is the (convex) plasticity criterion of the material. A field $\sigma$ that is SA and PA will be said to be (fully) admissible.

Similarly, a strain rate tensor field $v$ is kinematically admissible (KA) if it is derived from a continuous velocity vector field $u$ such that the velocity boundary conditions are verified. It is said to be plastically admissible (PA) if the so-called associated flow (or normality) law is verified; the fields $u$ and $v$, which are KA and PA, will be called admissible.

A solution to the LA problem is a pair of fields $(\sigma, v)$ where $\sigma$ and $v$ are both admissible and associated by the normality law. Classically, these solutions can be found or approached using two optimization methods. The first one, involving only stresses as variables, is the statical (or lower bound) method. The second one, involving only displacement velocities as variables, is the kinematical (or upper bound) method.

Another approach, the so-called mixed approach, involving stresses as real variables and displacement velocities as virtual variables, results in an optimization problem of the same form as for the lower bound approach. In the following we use this method modified to give true kinematical bounds as detailed in [9], for it is very appropriate to the proposed decomposition approach.

### 2.2. Formulation of the variational mechanical problem

Let us consider a KA virtual velocity field $u$. The virtual power principle (VPP) states that the stress tensor fields $\sigma$ and the load vector $Q$ are in equilibrium, if, *for any* KA $u$, the following equation is verified:

$$P_{\text{ext}} = Q \cdot q(u) = \int_V \sigma : v \, \mathrm{d}V, \tag{1}$$

where $V$ is the volume of the mechanical system. In (1) we have assumed, as in [10], that the power of the external forces can be written as the scalar product of a loading vector $Q$ and a generalized velocity vector $q(u)$, which is linear in $u$.

After some change, the mixed kinematical formulation of [5] becomes the following variational mechanical problem:

$$\max_{Q,\,\sigma} F = Q \cdot q^d \tag{2a}$$

$$\text{s.t.} \; -\int_V \sigma : v \, \mathrm{d}V + Q \cdot q(u) = 0 \quad \forall \,\text{KA}\, u, \tag{2b}$$

$$f(\sigma) \leqslant 0, \tag{2c}$$

where $q^d$ is a fixed value of $q(u)$. In (2) *any* velocity and stress fields must be taken into account. Indeed, this is not the case when we consider a discretization of the mechanical system in finite elements, obtaining in fact only estimates of the limit loads. In [3,9] the following numerical form of the variational mechanical problem (2) is proved to give a strict upper bound to the limit load, in the linear as well as in the quadratic case:

$$\text{Max}\{q^d\}^{\mathrm{T}}\{Q\} \tag{3a}$$

$$\text{s.t.} \; -[\alpha]\{\sigma\} + [\beta]\{Q\} = 0, \tag{3b}$$

$$f(\sigma) \leqslant 0 \quad \text{at all apexes.} \tag{3c}$$

where the matrices $[\alpha]$ and $[\beta]$ result from the calculation of the variational equation (2b) over the finite element mesh and its discontinuous velocity fields.

With $A = [-[\alpha], [\beta]\,]$, $b = 0$, $x^{\mathrm{T}} = \{\{\sigma\}^{\mathrm{T}}, \{Q\}^{\mathrm{T}}\}$ and $g(x) = f(x)$, this problem has the following simplified form:

$$\begin{array}{ll} \max & c^{\mathrm{T}} x \\ \text{s.t.} & Ax = b, \\ & g(x) + s = 0, \quad s \geqslant 0. \end{array} \tag{4}$$

## 3. Interior point method and convex optimization

The paper [2] details a nonlinear algorithm for solving the plane strain statical problem of Limit Analysis (LA) for both von Mises and Gurson materials, implemented in IP-OPT. The optimization problems present a linear objective function and a mix of linear and nonlinear convex constraints. For problems where the plasticity criterion is the von Mises or Drucker–Prager criterion, the nonlinear constraints are convex quadratic inequalities, making the problems second-order conic programming problems for which specific codes exist. Unfortunately, these codes do not provide enough accuracy

when postanalyzing the solutions, at least in the kinematical case presented herein, resulting in nonadmissible solutions for our large-scale problems. The IP-OPT code has overcome this drawback, as it appears to be limited only by the RAM addressability of the 32-bits version of MATLAB we used on an Apple MacPro for the present calculations.

The general form of the optimization problems to be solved here is as follows:

$$\begin{array}{ll} \max & c^{\mathrm{T}}x \\ \text{s.t.} & Ax = b, \\ & g(x) + s = 0, \quad s \geqslant 0, \end{array} \tag{5}$$

where $c, x \in \mathbb{R}^n$, $b \in \mathbb{R}^m$, $A \in \mathbb{R}^{m\times n}$ is the matrix of the linear constraints, $g = (g_1, \ldots, g_p)$ is a vector-valued function of $p$ convex numerical functions $g_i$, and $s \in \mathbb{R}^p_+$ is the vector of slack variables associated with these convex constraints. This is precisely the kind of problem we had to solve in Section 2.2.

We solve, instead of the previous problem, the following one, parametrized by $\mu > 0$, the "barrier parameter":

$$\begin{array}{ll} \max & c^{\mathrm{T}}x + \mu \displaystyle\sum_{i=1}^{p} \ln(s_i) \\ \text{s.t.} & Ax = b, \\ & g(x) + s = 0, \quad s > 0. \end{array} \tag{6}$$

Thus, this problem can be tackled by the class of optimization methods known as "primal–dual interior point methods", which have recently proved to be more efficient than the approaches dealing directly with the original problem (5).

Following this primal–dual interior point method, the problem (6) has a solution if and only if the following conditions are satisfied:

$$\begin{aligned} & -c + A^{\mathrm{T}}w + \left(\frac{\partial g}{\partial x}\right)^{\mathrm{T}} y = 0, \\ & Ax - b = 0, \\ & g(x) + s = 0, \\ & YSe = \mu e, \end{aligned} \tag{7}$$

where $w \in \mathbb{R}^m$, $y \in \mathbb{R}^p$, $e = [1 \ldots 1]^{\mathrm{T}} \in \mathbb{R}^p$ and $Y, S$ are the diagonal matrices associated with $y$ and $s$, respectively; $\mu > 0$ and $s > 0$ imply $y > 0$.

For each given $\mu$, the nonlinear system (7) is approximately solved by one iteration of the Newton method, thereby providing an approximate solution of the parametrized problem (6). Using a sequence of values for $\mu$ decreasing to zero, we make the latter converge to the solution of (2). Indeed, as $\mu$ approaches zero, Eq. (7) come close to the KKT conditions for the original problem. The code and its MATLAB implementation are fully detailed in [3].

## 4. The proposed decomposition method

The present decomposition approach is based on a partition of the FEM mesh, however with no real connection with the so-called domain decomposition methods. Moreover, the latter appear not to be applied to optimization problems, as can be seen in the very complete reference [11] presenting the state of the art on the domain decomposition approaches.

As regards the limit analysis problem, to our knowledge, the domain decomposition approach was only used in [12] for a classical kinematical approach, with nonoverlapping subdomains. However, no details are given on how the variable values are updated at the interfaces from one iteration to another. *A contrario*, the present method proceeds iteratively with an auxiliary problem for each interface at each decomposition level in order to upgrade the interface velocities; moreover, a few iterations are necessary in fact. Hereafter we present the method and then its application to two standard mechanical problems.

The method was first developed in continuous, piecewise linear velocity; it is exemplified in plane strain with the problem of a bar compressed under rough rigid plates with a ratio width versus height $b/h$ equal to 2 (Fig. 1). Given the symmetries of the problem, only the left upper quarter of the bar is meshed in $4 \times 2$ squares or rectangles diagonally subdivided into four triangles. The velocities vary continuously and piecewise linearly. The rigid plate goes down with a uniform, vertical velocity $U_0$, which is created through the action of a central vertical force $F$ to be determined. The isotropic, homogeneous material obeys the von Mises (or Tresca) criterion with cohesion $c$. A simple four-blocks mechanism for the problem gives $F/(bc) = 2.5$, and the exact solution is attributable to Salençon [13], namely 2.42768 in the present case. The velocities of the bar and the plate at the interface are the same, i.e., no sliding is allowed so that the dissipated power is only volumic. Here, there is only one loading parameter $Q = F$ and the generalized associated velocity is $q^d = U_0$; both will be the same for all subproblems because of a vertical partition of the mesh; this is a fair feature, as will be seen in the second problem where the loading factor is the specific weight.

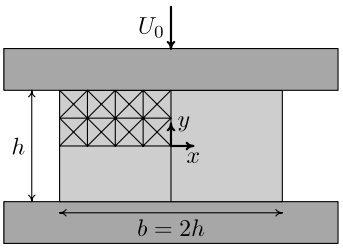


**Fig. 1.** The compressed bar, $b = 2h$, mesh $2N \times N$, here $N = 2$.

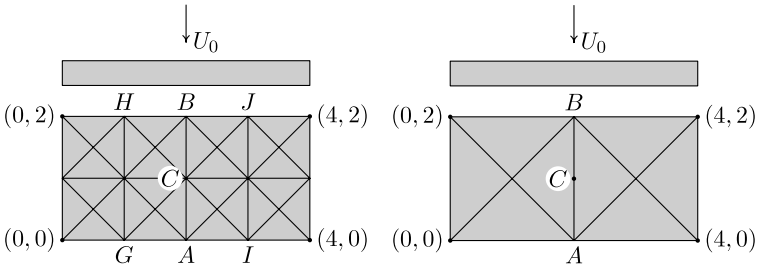


(a) Target problem. (b) Starting problem.

**Fig. 2.** The starting and target meshes.

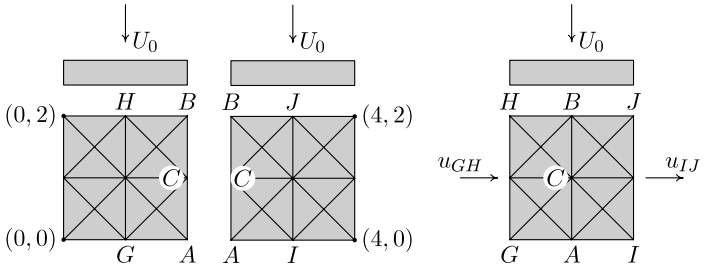


(a) The left problem. (b) The right problem. (c) The middle problem.

**Fig. 3.** Problems II and problem III.

### *4.1. The starting problem*

Solving first this reduced problem provides a good initialization for the velocities at the separating interface $AB$ of the target problem (Fig. 2a) using an appropriate interpolation.

Another solution would consist in extracting the interface values from an analytical kinematical solution; however, this technique, generally less efficient in terms of convergence rate, also requires a preliminary treatment specific to the mechanical problem considered. Hence, the $2 \times 1$ problem of the same bar problem is solved first (Fig. 2b).

The solution of this starting problem gives the initial nodal values at the points $A$, $B$, $C$, i.e., $u^A$, $u^B$ and $u^C$, which will be taken as boundary conditions, in fact as new kinematical parameters $q_i^d$ for the left ($\text{II}_\text{l}$) and the right ($\text{II}_\text{r}$) subsequent problems II. The velocity of the point $C$ is calculated by linear interpolation, because of the linear variation of the velocity inside the triangles. Note finally that a complete starting solution could also be extrapolated for the two following subproblems, but it is well known that this possibility is much less efficient in the present interior point method than in linear programming; hence, it was not tested here.

### *4.2. The "left" and "right" problems*

The meshed subproblems are presented in Fig. 3. We note the lengths of the sides $AC$ and $BC$ as $l_{AC}$ and $l_{BC}$, the values of $\sigma_{xx}$ and $\sigma_{xy}$ on the side $AC$ as $p_{AC}$ and $t_{AC}$, respectively, and $p_{BC}$ and $t_{BC}$ their values on the side $BC$. These stress components are considered constant on their sides because constant stress tensors in the triangles are needed here to keep the kinematical properties.

*4.2.1. The left problem II*

Let us now make explicit the power of the external forces $P_{\text{ext}}$, (Fig. 3a):

$$\begin{aligned} P_{\text{ext}} &= FU_0 + \int_{AC} pu_x \,\mathrm{d}y + \int_{CB} pu_x \,\mathrm{d}y + \int_{AC} tu_y \,\mathrm{d}y + \int_{CB} tu_y \,\mathrm{d}y \\ &= FU_0 + p_{AC} l_{AC} \frac{u_x^A + u_x^C}{2} + p_{CB} l_{CB} \frac{u_x^C + u_x^B}{2} + t_{AC} l_{AC} \frac{u_y^A + u_y^C}{2} + t_{CB} l_{CB} \frac{u_y^C + u_y^B}{2}. \end{aligned} \tag{8}$$

By reordering (8) we obtain seven generalized velocities $q_i^d$ which are the six components of the velocities at the points $A$, $B$, $C$, and $U_0$ as expected. Then we define the functional of the left problem (Fig. 3a) as:

$$P_{\text{ext}} = FU_0 + Q_1 u_x^A + Q_2 u_y^A + Q_3 u_x^C + Q_4 u_y^C + Q_5 u_x^B + Q_6 u_y^B. \tag{9}$$

In fact, the equality between $q(u)$ and $q^d$ in the optimal solution will lead to the expected verification of the new boundary conditions. Relation (9) gives the functional to be maximized for the problem $\text{II}_\text{l}$: it will be noted $FU_0 + Q_i q_i$ using the usual Einstein convention with $i = 1 \ldots 6$.

In the second example (discontinuous quadratic velocities), the present mesh would have six nodes on the interface, giving rise to 13 final loading parameters by assuming an affine distribution of the stress vector.

*4.2.2. The right problem II*

This time the velocities $u^A$, $u^B$, $u^C$ are imposed at the left side of the mesh in Fig. 3b. This problem is analogous to the preceding one, except for the appearance of symmetry at the right side. As previously, we have, after reordering:

$$P_{\text{ext}} = FU_0 + Q_1' u_x^A + Q_2' u_y^A + Q_3' u_x^C + Q_4' u_y^C + Q_5' u_x^B + Q_6' u_y^B = FU_0 + Q_i' q_i. \tag{10}$$

Joining all the interface nodal points of the $\text{II}_\text{l}$ and $\text{II}_\text{r}$'s optimal solutions gives an admissible solution for the entire problem, i.e., the target problem: the dissipated power is the sum of the subproblem's dissipated power, giving a target functional value lower than (or at least equal to) the value of the starting problem.

In order to progress by iterating the process, upgrading the velocities at the interface is obviously necessary; hence the idea of the following specific phase III is to improve these interface values.

*4.2.3. The problem III*

Prior to this phase, the optimal values along the $GH$ segment obtained in the $\text{II}_\text{l}$ problem and the values along $IJ$ in $\text{II}_\text{r}$ are saved in an external file. The solution to problem III (Fig. 3c) is obtained as in the previous problem, except that the new loading parameters are now defined from the lateral sides $GH$ and $IJ$ (here a total of 13 parameters); the updated values at the central interface $AB$ correspond to a lower dissipated power in the $GHJI$ mesh. Note that at this stage, combining (by postanalysis) the field of the left half part of $\text{II}_\text{l}$ and the field of right half part of $\text{II}_\text{r}$ with the field of the present phase gives an admissible field for the target problem, with a dissipated power lower than the previous value.

Finally, by going back to phase II with the new values on $ACB$, the process can be resumed. Each following iteration, namely a global one, consists in solving the problems III, $\text{II}_\text{l}$ and $\text{II}_\text{r}$.

## 5. Validation and exploitation

The proposed decomposition approach was first investigated for the compressed bar for continuous velocities and then for the classical problem of a vertical slope in the discontinuous quadratic case. This last problem is a difficult one, because it results in large-scale optimization problems and requires a high level of precision – and meticulous postanalysis of the solution fields – in order to guarantee the final numerical value of the optimal loading parameter.

### 5.1. The compressed bar problem

*5.1.1. First-level decomposition*

Let us now consider a $64 \times 32$ target problem and a $32 \times 16$ starting problem. These meshes were selected as a good compromise between efficiency and CPU time in accordance with the number of calculations to be made for these validation tests. Moreover, it is worth recalling the absence of locking problems in this mixed approach, unlike the classical approach.

Fig. 4 illustrates the progression of the loading parameter $F/c$ from the starting value 159.01, (i.e., $F/(bc) = 2.4845$, with $b = 64$ and $c = 1$) versus the iteration number to the final value: 157.339. The three subproblems (II and III) here are $32 \times 32$ problems. Solving the target problem directly gives the asymptotic value 157.33, the exact solution giving 155.37. Another first-level decomposition, where problem III is first solved after the starting problem and so on, gives a bit lower convergence value, but with no significant difference when the starting problem is more refined, as expected.

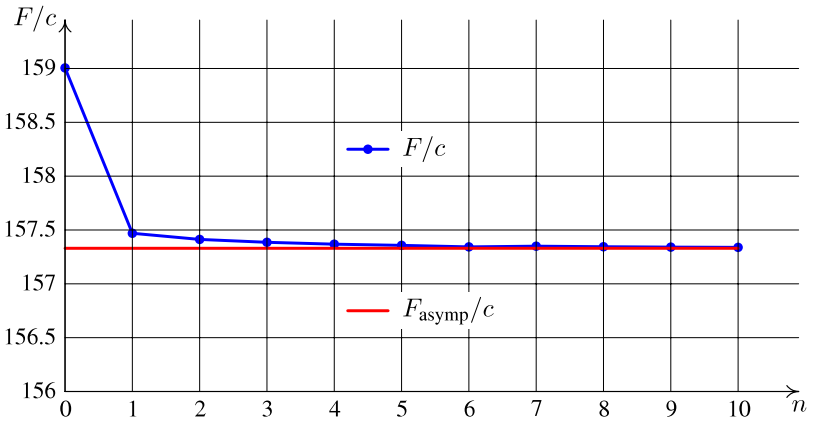


**Fig. 4.** Variation of $F/c$ related to the number of iterations $n$.

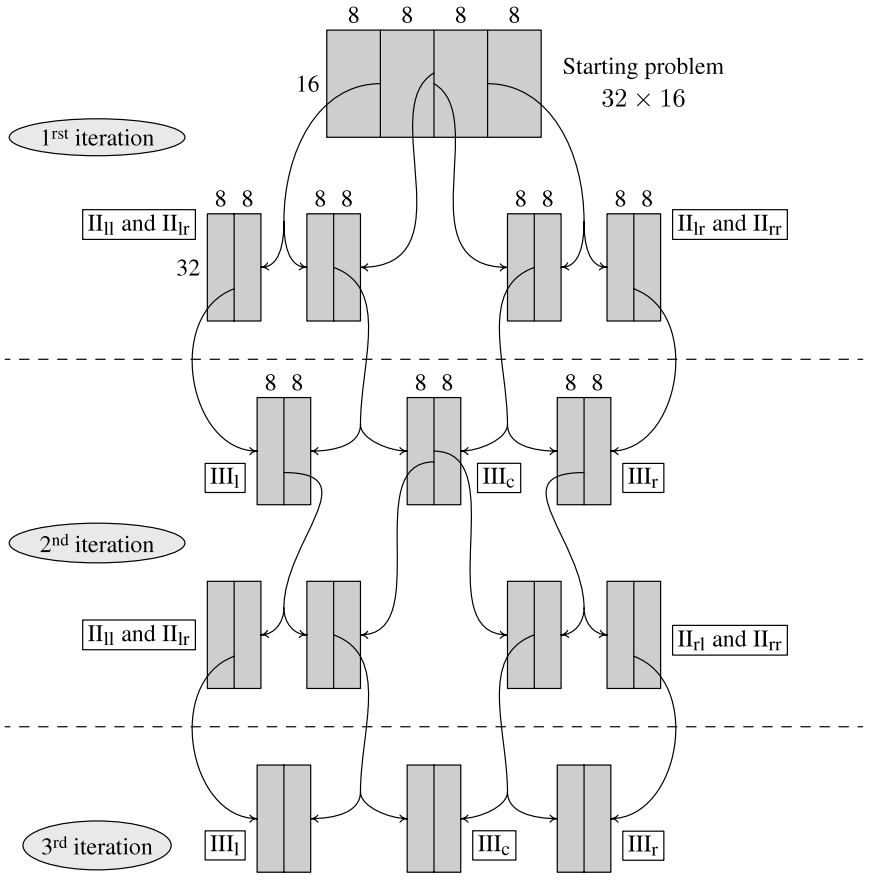


**Fig. 5.** Second-level decomposition of the 64 × 32 plate.

*5.1.2. Second-level decomposition*

The target problem is again the 64 × 32 problem, which gives the optimal value $F/c = 157.33$ in 1030 s of CPU time. Problems II are themselves subdivided into subproblems.

Problem $II_l$ produces subproblems $II_{ll}$ and $II_{lr}$ , problem $II_r$ yields subproblems $II_{rl}$ and $II_{rr}$. Consequently, three problems III are defined: $III_l$ for problems $II_{ll}$ and $II_{lr}$, $III_r$ for problems $II_{rl}$ and $II_{rr}$, and finally a central $III_c$ to update the central interface. The whole process is illustrated in Fig. 5.

The final result (157.463) from Table 1 must be compared to the result obtained after the first iteration of the first-level decomposition, i.e., 157.469 in 533 s, the target problem giving 157.33 in 1033 s.

**Table 1**
Compressed bar 64 × 32: results of the second-level decomposition.

| Iteration | 1 | Iteration | 2 | 3 | 4 |
|---|---|---|---|---|---|
| | | $III_l$ | 41.7815 | 41.7128 | 41.6814 |
| Starting | 159.0051 | $III_r$ | 36.6723 | 36.6817 | 36.6915 |
| | | $III_c$ | 41.5183 | 41.5467 | 41.5486 |
| Time | 66 s | Time | 343 s | 387 s | 70 s (start. point) |
| $II_{ll}$ | 33.4242 | $II_{ll}$ | 42.3162 | 42.2861 | 42.2724 |
| $II_{lr}$ | 40.1507 | $II_{lr}$ | 41.6370 | 41.6215 | 41.6215 |
| $II_{rl}$ | 41.5851 | $II_{rl}$ | 40.1323 | 40.1462 | 40.1462 |
| $II_{rr}$ | 42.4637 | $II_{rr}$ | 33.4320 | 33.4309 | 33.4309 |
| $F_{tot}$ | 157.6238 | $F_{tot}$ | 157.5176 | 157.4847 | 157.4627 |
| Time | 350 s | Time | 430 s | 357 s | 243 s (start. point) |

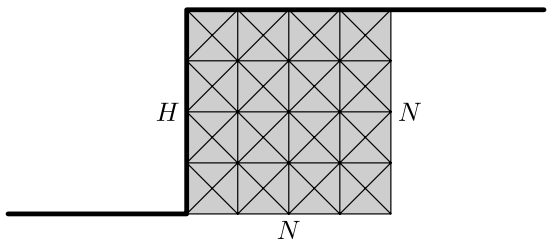


**Fig. 6.** The vertical slope with an $N = 4$ mesh.

It can be seen that four level-2 iterations are necessary to improve the value obtained at the first level-1 iteration, using the same starting problem in both cases. Also, at the iteration 4 we have used the complete solution of iteration 3 as a starting point for the optimization algorithm, resulting in less CPU time: we can see that this possibility should actually be used right from the first iteration. This efficiency comes from the fact that only the functional changes from one iteration to another in this mixed approach.

### *5.2. The vertical slope problem*

#### *5.2.1. Position of the problem*

This time the decomposition method is applied, using the discontinuous quadratic model, to the vertical slope problem in a von Mises/Tresca material, the height of which is noted $H$, the specific weight $\gamma$ and the cohesion $c$. The best known upper bound for the loading parameter $\gamma H/c$ (named safety factor in geotechnics) was given as 3.782 in [14], the best lower bound as 3.7752 recently in [15]. The mesh is square with $N \times N$ rectangles of four triangles each, as depicted in Fig. 6 for $N = 4$.

First, a global, coarser mesh is optimized by a power law acting on the coordinates in order to concentrate the mesh at the bottom of the slope. Then the optimized mesh is divided into horizontal slices of the same number of elements.

In the present case, let $q_\gamma = \int u_y \, dS$ and $Q_\gamma = \gamma$, where the axis $y$ is vertical. The generalized velocity $q_\gamma$ is not the same for all subproblems, contrary to the previous compressed bar where the plate acted on all subproblems with the same velocity. *Via* the (systematic) postanalysis, at each step the subproblem $i$ has its quota of $q_\gamma$ imposed – i.e., $q^d_{\gamma i}$ – obtained from the solution fields of the previous step, as the interface velocities; indeed, the sum of the $q^d_{\gamma i}$ remains equal to the initial $q^d_\gamma$. The global mesh is an $N \times N$ square for all tests.

#### *5.2.2. Details of the tests*

The results of the tests (evolution of $\gamma H/c$ as a function of the size of the mesh) are shown in Fig. 7.

From $N = 16$ to 96, the problem is solved directly. It is worth noting that only the IP-OPT solver has converged to an optimal solution beyond the $N = 70$ case, contrary to commercial codes in this problem. Then, from $N = 100$ to $N = 120$, the problem was divided into two subproblems in a level-1 decomposition.

For $N = 120$, two iterations were performed (starting–$II_{top}$–$II_{bottom}$, then III–$II_{top}$–$II_{bottom}$), and the results were the following:

- starting problem ($N \times N = 60 \times 60$) : $\gamma H/c = 3.7813$;
- iteration 1 : $\gamma H/c = 3.7789$;
- iteration 2 : $\gamma H/c = 3.7788$.

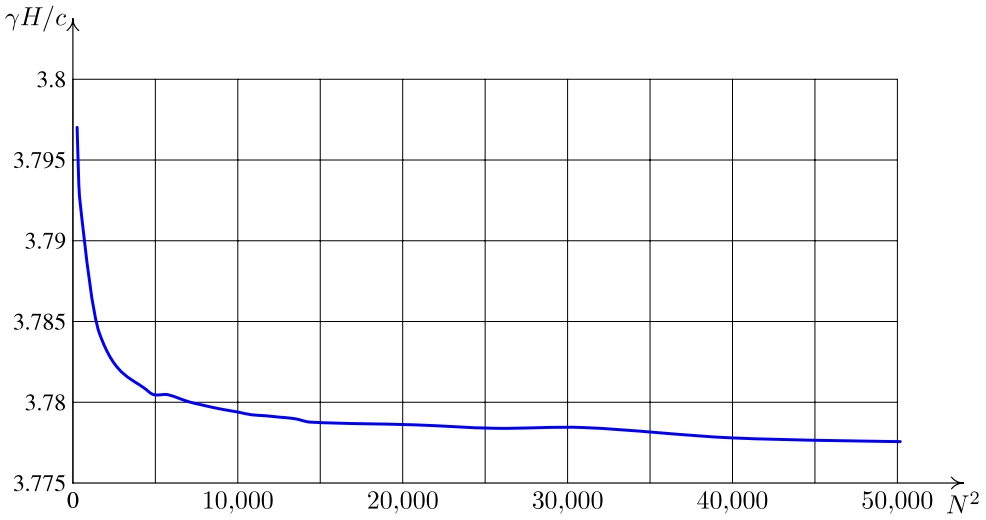


**Fig. 7.** The vertical slope: $\gamma H/c$ versus the size of the mesh.

Clearly, at least for this problem where the decomposition approach was intensively tested, the first iteration is sufficient if the subproblem meshes are well refined. This should be due to the discontinuous character combined with the quadratic variation of the velocities, solved without any problem using the IP-OPT solver in all cases.

For $N = 144$, 160, 176, 200 and 224, both subproblems were themselves decomposed in a level-2 decomposition. The final optimal $224 \times 224$ value was $\gamma H/c = 3.7776$. In fact, in postanalysis, the dissipated power is also recalculated using the analytical $\pi$ functions, lowering the IP-OPT value from 3.77764 to 3.77756, with all verifications better than $10^{-6}$ in all subproblems: this confirms the previously mentioned efficiency of the present mixed method in spite of optimizing an upper bound to the real dissipated power.

For $N = 200$ and $N = 224$, the problem was replaced, as in [16], by an equivalent problem, such that the soil is weightless and the boundary conditions are defined by $\sigma_n = \gamma h$, $\tau_{nt} = 0$, $h$ denoting the depth measured from the upper surface. The CPU times vary from 6 to 14 h for the four subproblems of the $N = 224$ problem.

To be complete, let us note that the target $224 \times 224$ problem (200,704 quadratic discontinuous triangles) should give a problem with 3613,120 variables and 1806,800 linear constraints plus 1204,240 nonlinear ones!

## 6. Conclusion

The proposed decomposition method makes full use of the specific features of the mixed but totally kinematical approach. Its remarkable efficiency lies in fact in the constant robustness and the rapidity of the IP-OPT solver under MATLAB. Indeed, it can be used with non-regular meshes, providing the interfaces are really common in terms of nodal points and variation velocity in order to keep the kinematic character of the final results.

In the present kinematic approach, from the first iteration the accuracy of the final optimum is good, with steady improvement during the following iterations. Hence, using a refined starting problem, we can iterate the decomposition process, here to level 2, and obtain very good and accurate solutions for meshes that are not directly within reach, especially for open problems where a fine bracketing of the solution still exists. For example, in the vertical slope problem, we were able to lower the upper bound from 3.782 to 3.7776 by decomposing an optimization problem that was directly intractable until now, a result that should be evaluated by comparison with the very recent lower bound 3.7752 of [15], where the method is successfully extended to static case.

## Acknowledgements

Our final words will be to thank Pr. Joseph Pastor, from Université de Savoie, France, for his very valuable contribution to all the tests and results exposed in this article.

## References

[1] F. Pastor, Résolution d'un problème d'optimisation à contraintes linéaires et quadratiques par une méthode de point intérieur: Application à l'Analyse Limite, Mémoire de DEA de mathématiques appliquées, Université de Lille 1, 2001.
[2] F. Pastor, E. Loute, Solving limit analysis problems: An interior-point method, Commun. Numer. Methods. Eng. 21 (11) (2005) 631–642.
[3] F. Pastor, Résolution par des méthodes de point intérieur de problèmes de programmation convexe posés par l'analyse limite, Thèse de doctorat, Facultés universitaires Notre-Dame de la Paix de Namur, Département de mathématiques, 2007.

[4] M. Capurso, Limit analysis of continuous media with piecewise linear yield conditions, Meccanica 1 (1971) 53–58.
[5] E. Anderheggen, H. Knopfel, Finite element limit analysis using linear programming, Internat. J. Solids Structures 8 (1972) 1413–1431.
[6] D. Radenkovic, Q.S. Nguyen, La dualité des théorèmes limites pour une structure en mat'eriau rigide-plastique standard, Arch. Mech. 24 (5–6) (1972) 991–998.
[7] E. Christiansen, Limit analysis of collapse states, in: P.G. Ciarlet, J.L. Lions (Eds.), Handbook of Numerical Analysis, 1996, pp. 193–312.
[8] F. Pastor, M. Trillat, J. Pastor, E. Loute, P. Thoré, Convex optimization and stress-based lower/upper bound methods for limit analysis of porous polymer materials, in: J. B. et al. (Ed.), 9th European Mechanics of Materials Conference, EMMC9, École des Mines de Paris - EDF, May 2006.
[9] F. Pastor, E. Loute, J. Pastor, M. Trillat, Mixed method and convex optimization for limit analysis of homogeneous Gurson materials: A kinematical approach, Eur. J. Mech. A Solids 28 (2009) 25–35.
[10] J. Salençon, Théorie de la plasticité pour les applications à la mécanique des sols, Eyrolles, Paris, 1974.
[11] O. Widlund, D. e Keyes, Domain decomposition methods in science and engineering XVI, in: Lectures Notes in Computational Science and Engineering, Springer, 2007.
[12] J. Huang, W. Xu, P. Thomson, S. Di, A general rigid-plastic/rigid-viscoplastic FEM for metal-forming processes based on the potential reduction interior point method, Int. J. Machine Tools Manufacture 43 (2003) 379–389.
[13] J. Salençon, Théorie des charges limites: Poinçonnement d'une plaque par deux poinçons symétriques en déformation plane, Comptes Rendus Mécanique, Acad. Sci. Paris 265 (1967) 869–872.
[14] J. Pastor, E. Loute, T.H. Thai, Interior point optimization and limit analysis: An application, Commun. Numer. Methods. Eng. 19 (2003) 779–785.
[15] Z. Kammoun, F. Pastor, H. Smaoui, J. Pastor, A decomposition of the static problem in limit analysis, in: Euro-Mediterranean Symposium on the Advances in Geomaterials and Structures, AGS 2008, Hammamet, Tunisie, 2008, May 5–7.
[16] M. Frémond, J. Salençon, Limit analysis by finite-element methods, in: A.C. Palmer (Ed.), Proc. of Symposium on the Role of Plasticity in Soil Mechanics, Cambridge, England, 1973, pp. 297–308.